Free and Forced Vibrations of Monolithic and Composite Rectangular Plates With Interior Constrained Points

Arka P. Chattopadhyay
Department of Biomedical Engineering and Mechanics,
M/C 0219 Virginia Polytechnic Institute and State University,
495 Old Turner Street,
Blacksburg, VA 24061
e-mail: arka@vt.edu

Romesh C. Batra[1]
Honorary Fellow
Department of Biomedical Engineering and Mechanics,
M/C 0219 Virginia Polytechnic Institute and State University,
495 Old Turner Street,
Blacksburg, VA 24061
e-mail: rbatra@vt.edu

The restriction of deformations to a subregion of a system undergoing either free or forced vibration due to an irregularity or discontinuity in it is called mode localization. Here, we study mode localization in free and forced vibration of monolithic and unidirectional fiber-reinforced rectangular linearly elastic plates with edges either simply supported (SS) or clamped by using a third-order shear and normal deformable plate theory (TSNDT) with points on either one or two normals to the plate midsurface constrained from translating in all three directions. The plates studied are symmetric about their midsurfaces. The in-house developed software based on the finite element method (FEM) is first verified by comparing predictions from it with either the literature results or those computed by using the linear theory of elasticity and the commercial FE software ABAQUS. *New results include: (i) the localization of both in-plane and out-of-plane modes of vibration, (ii) increase in the mode localization intensity with an increase in the length/width ratio of a rectangular plate, (iii) change in the mode localization characteristics with the fiber orientation angle in unidirectional fiber reinforced laminae, (iv) mode localization due to points on two normals constrained, and (iv) the exchange of energy during forced harmonic vibrations between two regions separated by the line of nearly stationary points that results in a beats-like phenomenon in a subregion of the plate. Constraining translational motion of internal points can be used to design a structure with vibrations limited to its small subregion and harvesting energy of vibrations of the subregion.*

[DOI: 10.1115/1.4041216]

Introduction

Discontinuities and irregularities in a physical system may cause anomalies in its free and forced vibrations. Anderson [1] observed that irregularities in electrons distribution in different lattice structures vary their vibration characteristics and the material conductivity; this phenomenon is called *Anderson's localization* [2]. Hodges [2] extended the vibration localization phenomenon to continuous periodic structures. Subsequently, numerous works have illustrated the mode localization phenomenon in continuous structures that include periodic structures with cyclic symmetry [3–5], multispanned beams [6], and irregular structures [7–9].

Early works on mode localization in continuous bodies were mostly restricted to one-dimensional (1D) problems possibly because of difficulties in computing eigen-modes [8]. Hodges and Woodhouse [7], based on Herbert and Jones's work [9], used a statistical perturbation method to study localization phenomenon in a string by inducing an irregularity with a slidable mass. They found good agreement between their analytical and experimental results. Depending on the magnitude of internal coupling of the structure, they divided the localization phenomenon into weak and strong. Using a mathematical model closely related to Kirkman and Pendry's [10] solid state physics model, Pierre [8] delineated factors for the weak and the strong localization phenomena.

Pierre and Plaut [11] used the perturbation approach to study the mode localization phenomenon in multispan hinged beams. Due to mathematical similarities between the free vibration and the elastic buckling problems, one can also observe the mode localization phenomenon in elastic buckling of thin structures. For example, Nayfeh and Hawwa [12] used principles of mode localization to control buckling of structures, and Paik et al. [13] characterized buckling localization in composite laminae with constrained interior points. Ibrahim [14] as well as Hodges and Woodhouse [15] have reviewed the literature on the localization phenomenon published till 1987.

Nowacki [16] analytically studied, using a Levy solution, vibration of simply supported (SS) rectangular plates with multiple internal constrained points. Gorman [17] analytically investigated free vibrations of plates clamped only at symmetric points on the diagonals and used a plate theory. Gorman and Singal's [18] experimental findings agreed well with the analytical results of Ref. [17].

Bapat et al. [19,20] and Bapat and Suryanarayan [21,22] employed the flexibility function approach to study free vibration of point supported plates. Bapat and Suryanarayan [23] extended it to analyze mode localization in SS rectangular plates having internal constrained points. Lee and Lee [24] adopted the impulse function approach to analytically solve similar problems.

Rao et al. [25], Raju and Amba-Rao [26], and Utjes et al. [27], among others, have numerically analyzed the mode localization phenomenon in rectangular plates with point supports by using the finite element method (FEM), whereas Kim and Dickinson [28] and Bhat [29] used the Rayleigh–Ritz method. Filoche and Mayboroda [30] used the Kirchhoff plate theory and the FEM to show that constraining all points on a normal to the plate midsurface of a rectangular plate induced strong mode localization. Sharma et al. [31] used a first-order shear deformation theory (FSDT) and the FEM to show the mode localization phenomenon in composite rectangular plates when both bending and transverse

[1]Corresponding author.

Contributed by the Technical Committee on Vibration and Sound of ASME for publication in the Journal of Vibration and Acoustics. Manuscript received June 10, 2018; final manuscript received August 9, 2018; published online September 17, 2018. Assoc. Editor: Julian Rimoli.

shear deformations are incorporated in the analysis. These studies [30,31] considered only bending or out-of-plane modes of vibration, and all plate edges clamped. It seems that the localization of in-plane modes of vibration, effects of SS edges on mode localization, and constraining points on two normals to the plate mid surface have not been scrutinized. For SS plates, Batra and Aimmanee [32] analytically found these and bending vibration modes by using complete polynomials in the Levy type solutions. Other authors have studied either in-plane (e.g., see Ref. [33]) or bending (e.g., see Ref. [34]) modes of vibration only. Even though one can study mode localization by separately using the bending and the stretching plate theories and then combining the results, the use of a third-order shear and normal deformable plate theory (TSNDT) simultaneously gives both types of modes. It thus does not require studying the problem with two different plate theories. The TSNDT does not require a shear correction factor, frequencies and mode shapes of the first 100 modes of vibration agree well with those computed using the linear elasticity theory (LET), and the in-plane stresses computed from the TSNDT displacements and the constitutive relation agree well with those found using the LET. Furthermore, the transverse stresses computed by using a one-step stress recovery scheme are close to those obtained using the LET. For materials with Poisson's ratio close to 0.49, the transverse normal strains are likely to be of the same order of magnitude as the axial strains and require plate theories that consider transverse normal strains.

The TSNDT is particularly useful for problems involving inhomogeneous materials with elastic moduli varying along the plate thickness. Vel and Batra [35] showed that many simple plate theories do not predict well stresses at critical locations. As demonstrated by Shah and Batra [36], the TSNDT solution provides reasonably accurate values of stresses everywhere in the plate.

Here, we study the mode localization phenomenon in free and forced vibrations of monolithic and unidirectional fiber-reinforced laminated rectangular linearly elastic plates with internal constrained points by using a TSNDT. Lo et al. [37], Carrera [38], Vidoli and Batra [39], and Batra and Vidoli [40], among others, have proposed higher-order shear and normal deformable plate theories based on Mindlin's classical work [41]. As also observed in Refs. [30] and [31] who did not consider transverse normal deformations, with an increase in the length/width ratio for a rectangular plate, the mode localization becomes stronger. One of the new results reported here is the mode localization for in-plane modes of vibration. We show that the first 100 frequencies and strain energies associated with their mass normalized mode shapes computed by using the TSNDT agree well with those found from the LET. Subsequently, we compute results with the TSNDT and study mode localization in both isotropic and composite plates. We also study forced vibrations of internally constrained plates to delineate if vibrations are localized.

For forced harmonic vibrations of an internally constrained plate at a frequency close to that of the mode for which vibrations are localized in one of the two regions, the response strongly depends upon which region exhibited mode localization. For example, we observe beats like phenomenon in the shorter region of the plate possibly due to the energy transfer between the two regions. This is similar to the steady-state response observed in Refs. [42] and [43] in structures composed of vibration absorbing dampers. Spletzer et al. [44] have used this principle to design ultrasensitive mass sensors using linked cantilever beams. Thus, the mode localization phenomenon can be both beneficial and harmful based on design requirements. It serves as a tool for designing structures with desired vibration characteristics.

Problem Formulation

We use both the LET and a TSNDT to analyze free and forced infinitesimal vibrations of linearly elastic rectangular plates with and without constraining interior points on either one or two normals to the plate midsurface. A schematic sketch of the problem studied is exhibited in Fig. 1 wherein rectangular Cartesian coordinates, used to describe plate's deformations, are also depicted.

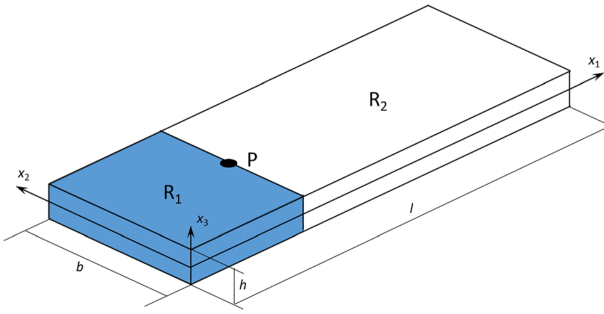

Fig. 1 Schematic representation of a rectangular plate with the rectangular Cartesian coordinate axes. Points on the normal through the point *P* may be constrained from translating in all three directions.

The Linear Elasticity Theory. For the LET, equation governing deformation of a plate in the absence of body forces is

$$\rho \ddot{u}_i = \sigma_{ij,j} \tag{1}$$

where $u_i (i = 1, 2, 3)$ is the displacement along the x_i-axis, $\sigma_{ij,j} = \partial\sigma_{ij}/\partial x_j$, σ_{ij} is the stress tensor, $\ddot{u}_i = \partial^2 u_i/\partial t^2$, t is the time, and a repeated index implies summation over the range of the index. Equation (1) is supplemented with Hooke's law

$$\sigma_{ij} = C_{ijkl}\varepsilon_{kl} \tag{2}$$

strain–displacement relations

$$\varepsilon_{ij} = (u_{i,j} + u_{j,i})/2 \tag{3}$$

and initial/boundary conditions

$$\begin{gathered} u_i(x_1, x_2, x_3, 0) = u_i^0(x_1, x_2, x_3), \dot{u}_i(x_1, x_2, x_3, 0) = \dot{u}_i^0(x_1, x_2, x_3) \\ \sigma_{ij}n_j = t_i(x_1, x_2, x_3, t) \text{ on } \Gamma_t, \\ u_i(x_1, x_2, x_3, t) = u_i^{bc}(x_1, x_2, x_3, t) \text{ on } \Gamma_u \\ \Gamma_t \cup \Gamma_u = \partial\Omega, \Gamma_t \cap \Gamma_u = \phi \end{gathered} \tag{4}$$

Here Γ_t and Γ_u are, respectively, parts of the boundary where surface tractions and displacements are prescribed as $t_i(x_1, x_2, x_3, t)$ and $u_i^{bc}(x_1, x_2, x_3, t)$, $\boldsymbol{n}$ is a unit outward normal to Γ_t, $u_i^0(x_1, x_2, x_3)$ is the initial displacement field, $\dot{u}_i^0(x_1, x_2, x_3)$ is the initial velocity field, and Ω is the region occupied by the plate. We note that linearly independent components of $u_i(x_1, x_2, x_3, t)$ and $\sigma_{ij}n_j$ can be prescribed at a point on the plate surfaces. Substitution from Eqs. (2) and (3) into Eq. (1) results in three coupled linear partial differential equations for finding u_i. At an interior constrained point $(\bar{x}_1, \bar{x}_2, \bar{x}_3)$, we set $u_i(\bar{x}_1, \bar{x}_2, \bar{x}_3, t) = 0$.

Third-Order Shear and Normal Deformable Plate Theory. In the TSNDT, the displacement field is approximated as

$$u_i(x_1, x_2, x_3, t) = \sum_{j=0}^{3} (x_3)^j u_{ij}(x_1, x_2, 0, t), \quad i = 1, 2, 3 \tag{5}$$

where 12 functions, u_{ij}, are defined on the plate reference surface, here taken to be the plate midsurface, $x_3 = 0$. One may interpret u_{ij} as the jth order partial derivative of $u_i(x_1, x_2, x_3, t)$ with respect to x_3 evaluated at $x_3 = 0$. Alternatively, for $j = 1, 2, 3$, they can be interpreted as directors proposed by the Cosserat brothers [45].

Units of u_{ij} are length/(length)^j. Substituting for displacements from Eq. (5) into Eq. (1), we get

$$\rho(\ddot{u}_{i0} + x_3\ddot{u}_{i1} + x_3^2\ddot{u}_{i2} + x_3^3\ddot{u}_{i3}) = \sigma_{ij,j} \tag{6}$$

Multiplying both sides of Eq. (6) by $(x_3)^k$ $(k=0,\ 1,\ 2,\ 3)$ and integrating resulting equations with respect to x_3 over the plate thickness, we get

$$\sum_{j=0}^{3} A_{j+1}^{(k)}\ddot{u}_{ij} = \sum_{\alpha=1}^{2} M_{i\alpha,a}^{(k)} + ((x_3)k\sigma_{i3})|_{-h/2}^{h/2} - kM_{i3}^{(k-1)}, \quad i=1,2,3,\ k=0,1,2,\ \alpha=1,2 \tag{7}$$

where

$$\begin{aligned} A_j^{(k)} &= \int_{-h/2}^{h/2} \rho(x_3)^{k+j} dx_3,\ j=1,2,3,4 \\ M_{ij}^{(k)} &= \int_{-h/2}^{h/2} (x_3)^k \sigma_{ij} dx_3, \quad k=0,1,2,3 \end{aligned} \tag{8}$$

The element $A_j^{(k)}$ associated with $\ddot{u}_{ij}$ appears in the jth row and the kth column of the inertia matrix $\mathbf{A}$, and $M_{ij}^{(k)}$ is the kth order moment of σ_{ij} about the plate midsurface. $M_{ij}^{(0)}$ and $M_{ij}^{(1)}$, respectively, are the usual force per unit length and the moment per unit length; $M_{ij}^{(2)}$ and $M_{ij}^{(3)}$ are higher-order moments. Substitution from Eqs. (7), (2), and (3) into Eq. (8) gives expressions for $M_{ij}^{(k)}$ in terms of u_{ij}. These expressions when substituted in Eq. (7) yield 12 coupled linear partial differential equations for 12 unknown functions, u_{ij}.

Boundary conditions for the LET and the TSNDT at a clamped and a SS edge are listed below:

$$\begin{aligned} &\text{SS edge } x_1 = 0: \\ &u_2, u_3 = 0,\ \sigma_{11} = 0 \text{ for the LET;} \\ &\quad u_{2i}, u_{3i} = 0,\ M_{11}^{(i)} = 0,\ i = 0 \text{ to } 3 \text{ for the TSNDT} \\ &\text{Clamped edge } x_1 = 0: \\ &u_1, u_2, u_3 = 0 \text{ for the LET;} \\ &\quad u_{1i}, u_{2i}, u_{3i} = 0,\ i = 0 \text{ to } 3 \text{ for the TSNDT} \end{aligned} \tag{9}$$

Boundary conditions (9) for a SS edge are the same as those employed by Srinivas et al. [46] in their analytical solution of a linearly elastic problem and are used when seeking a Levy type solution. Analytical solutions for static and wave propagation problems for arbitrary boundary conditions are given in Refs. [35,47], and [48].

Numerical Solution of the Problem. For the above-stated two initial-boundary-value problems, we first derive weak formulations by employing the Galerkin method, e.g., see Ref. [49]. We numerically solve the resulting equations by the FEM with the in-house developed software for the TSNDT equations and the commercial software, ABAQUS, for the LET equations. We note that in each case, the resulting equations are expressed in matrix form as

$$\mathbf{M}\ddot{\mathbf{d}} + \mathbf{K}\mathbf{d} = \mathbf{F} \tag{10}$$

where $\mathbf{M}$ and $\mathbf{K}$, respectively, represent the mass and the stiffness matrices, and $\mathbf{d}$ is the vector of nodal unknowns, three for a node in the LET and 12 for a node in the TSNDT. Nodes are distributed throughout the three-dimensional (3D) plate domain for the LET and only on the two-dimensional plate reference surface for the TSNDT. We employ eight-node brick elements with $2\times2\times2$ integration points in an element for the LET and four-node quadrilateral elements for the TSNDT with 2×2 integration points in an element. The mass and the stiffness matrices, and the load vector for the TSNDT are evaluated by employing seven uniformly spaced integration points in the thickness direction. The total number of degrees-of-freedom (DOFs) for the TSNDT is considerably less than that for the LET.

Free Vibrations. For the free vibration problem, $\mathbf{F}=0$, and $\mathbf{d}(t) = \mathbf{D}e^{i\lambda t}$, no initial conditions are needed, and boundary conditions (4) are such that no work is done by external forces. Equation (10) reduces to the following eigenvalue problem:

$$[\mathbf{M} - \lambda^2\mathbf{K}]\mathbf{D} = \mathbf{0} \tag{11}$$

The cyclic frequencies f_i (in Hz) of the plate are given by

$$f_i = \lambda_i/2\pi \tag{12}$$

The number of frequencies equals the number of unconstrained DOFs or the dimensionality of the vector, $\mathbf{d}$, minus the number of constraints including those on the plate edges.

Forced Vibrations. For the transient analysis, we use the conditionally stable, central-difference time integration scheme, and a lumped mass matrix in ABAQUS for the LET equations and the consistent mass matrix for the TSNDT equations. Because of the generalized displacements in the TSNDT, terms in the mass matrix have different dimensions. Thus, one cannot employ the row sum technique of lumping the mass matrix. By nondimensionalizing variables, one could potentially use a lumped mass matrix. The time integration scheme is stable when the time-step size, Δt, satisfies the condition

$$\Delta t \le \Delta t_{\text{critical}} = 2/\lambda_{\max} \tag{13}$$

where $\lambda_{\max}(\text{rad/s})$ is the largest natural frequency of the system. The eigenvector for each frequency is normalized with respect to the mass matrix in both the LET and the TSNDT.

The computation of stresses for the LET is straightforward. For determining in-plane stresses in the TSNDT, we find strains with the TSNDT displacements and then stresses from the constitutive relation. We use a one-step stress recovery scheme to compute the transverse (out-of-plane) stresses. That is, we integrate with respect to x_3 the LET equations of motion starting from the bottom surface. For $\alpha=1$ and 2

$$\sigma_{\alpha3}|_{x_3=z} = \sigma_{\alpha3}|_{x_3=-h/2} + \int_{x_3=-h/2}^{z} \left(p\ddot{u}_\alpha - \frac{\partial\sigma_{\alpha\beta}}{\partial x_\beta}\right)dx_3 \tag{14}$$

where $z=x_3$. For evaluating the integrand in Eq. (14) at a given point, we first find the in-plane stresses at centroids of nine elements surrounding the point, fit a complete quadratic polynomial to each component of the stress by the least squares method, differentiate the polynomial, and then substitute in it coordinates of the point. Having found stresses σ_{13} and σ_{23}, the equation of motion in the x_3-direction is integrated with respect to x_3 to find σ_{33} that requires knowing $\sigma_{3\alpha,\alpha}$ for different values of x_3.

Example Problems

Verification of the Third-Order Shear and Normal Deformable Plate Theory Software for Free Vibrations of Rectangular Plates

Comparison of the First 100 Frequencies. We first verify the in-house developed software by comparing the lowest five fundamental frequencies of a linearly elastic, homogeneous, and isotropic $100\,\text{mm}\times100\,\text{mm}\times10\,\text{mm}$ plate having Young's

Table 1 First five nondimensional frequencies, $\omega_n = \omega h\sqrt{\rho/E}$, of the 100 mm × 100 mm × 10 mm SS plate

Mode	TSNDT (present)	Srinivas and Rao [34]	Qian et al. [50]	Batra and Aimmanee [32]
1	0.0581	0.0578	0.0578	0.0578
2	0.1393	0.1381	0.1391	0.1391
3	0.1393	0.1381	0.1391	0.1391
4	0.1949[a]	—	0.1948[a]	0.1949[a]
5	0.1949[a]	—	0.1948[a]	0.1949[a]

[a]In-plane mode of vibration and ω equals λ used earlier.

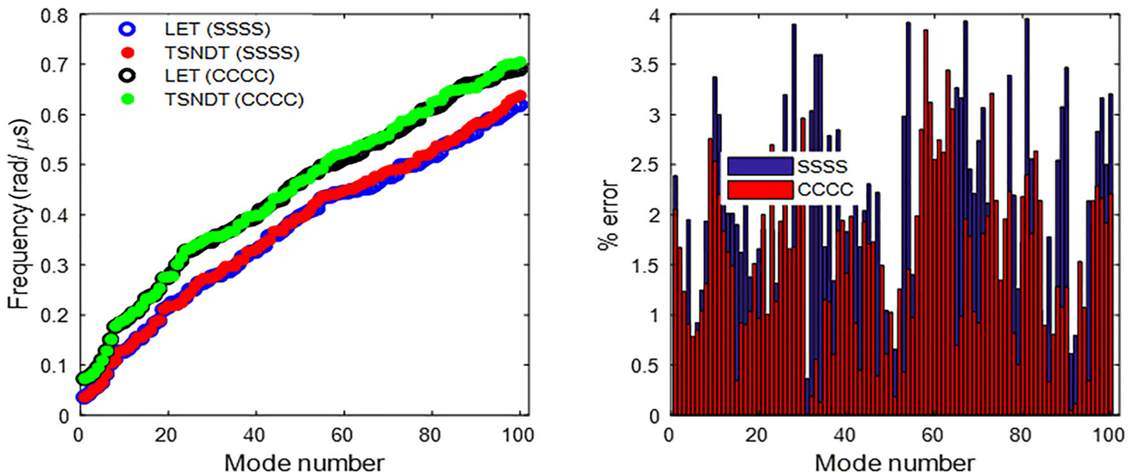

Fig. 2 First 100 frequencies, in rad/μs, from the TSNDT and the 3D LET (left), and the relative difference between them (right) for the 80 × 20 × 2 mm SS and clamped plates

modulus, $E = 200$ GPa, Poisson's ratio, $\nu = 0.3$, and mass density, $\rho = 7.2$ g/cc with their analytical values [34], and from higher order plate theories [32,50]. We successively refined the FE mesh of uniform elements for the TSNDT solution and found that the difference in the first ten frequencies using 40×40 (20,172 DOFs) and 30×30 elements (11,532 DOFs) was less than 1%. In Table 1, we have listed the presently computed first five converged frequencies using 40×40 uniform four-node elements and those found by other investigators. It is clear that the TSNDT predicted first five natural frequencies differ at most by 0.85% from their analytical values. We note modes 4 and 5 represent in-plane modes of vibration with $u_3 = 0$ that were absent from the analytical solution of Srinivas and Rao [34] since they considered only bending deformations.

When studying mode localization, we use first 100 frequencies. Accordingly, we now compare these computed from the TSNDT with those using the LET and the commercial FE software, ABAQUS. For the 80 mm × 20 mm × 2 mm (aspect ratio = length/thickness = 40) SS and clamped plates ($E = 25$ GPa, $\nu = 0.25$, $\rho = 5$ g/cc), we have exhibited in Fig. 2 the first 100 frequencies found from the two theories. When computing results using ABAQUS, we used $320 \times 80 \times 8$ uniform eight-node C3D8 elements resulting in 234,009 DOFs. The use of C3DR elements in ABAQUS did not give accurate frequencies of modes greater than 50. It is clear that the results from the two approaches differ by less than 4% for both the SS and the clamped plates. A similar exercise for the 80 mm× 20 mm× 4 mm (aspect ratio = 20) plate showed, respectively, the maximum difference of 2.3% and 3.8% for the SS and the clamped edges. Both the LET and the TSNDT gave several in-plane modes of vibrations.

Comparison of Strain Energies Associated With the First 100 Modes of Vibration. For mass normalized displacements for a mode shape $\mathbf{D}^T\mathbf{M}\mathbf{D} = 1$, $\mathbf{D}^T\mathbf{K}\mathbf{D}/2$ equals the strain energy of a linearly elastic body. Rayleigh's theorem (or premultiplying Eq. (11) by $\mathbf{D}^T$) gives

$$\lambda^2 = \mathbf{D}^T\mathbf{K}\mathbf{D}/\mathbf{D}^T\mathbf{M}\mathbf{D} \tag{15}$$

Thus, the strain energy of deformations associated with a mode shape equals one-half of the square of the frequency (in radians/s) of the mode shape. Because of the dimensional units used here, the strain energy in J equals 0.5 × (frequency in rad/μs)^2; we call this as the TSNDT (modal) energy.

One can also compute the strain energy, U, of a mode as

$$U = \frac{1}{2}\int_V \sigma_{ij}\varepsilon_{ij}dv \tag{16}$$

where stresses and strains are calculated from the mass normalized eigen-vectors; we call this as the TSNDT (direct) energy. We have exhibited in Fig. 3 strain energies associated with the first 100 modes from the two theories for the 80 mm × 20 mm × 2 mm plate for the SS and the clamped plates. These results evidence that the TSNDT and the LET give almost identical strain energies up to the first 50 modes and the TSNDT predicts slightly higher strain energies for the subsequent 50 modes.

Mode Localization in Clamped and Simply Supported Plates With Interior Constrained Points

Plates Made of Monolithic and Isotropic Materials. Following Ref. [30], we normalize rectangular plate's areal dimensions to $\sqrt{e} \times 1/\sqrt{e}$ to have unit surface area, and call e the eccentricity (it equals the length/width). We study its free vibrations with all points on the line, $x_1 = \sqrt{e}/5, x_2 = 1/2\sqrt{e}$ (i.e., normal to the plate midsurface through the point P $(\sqrt{e}/5, 1/2\sqrt{e}, 0)$, constrained or equivalently, restrained from translating in all three

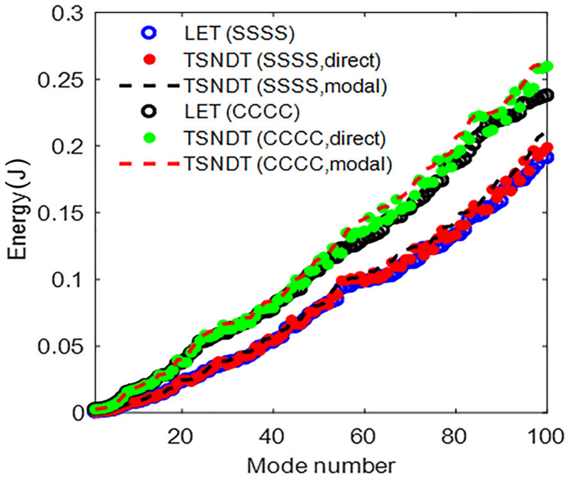

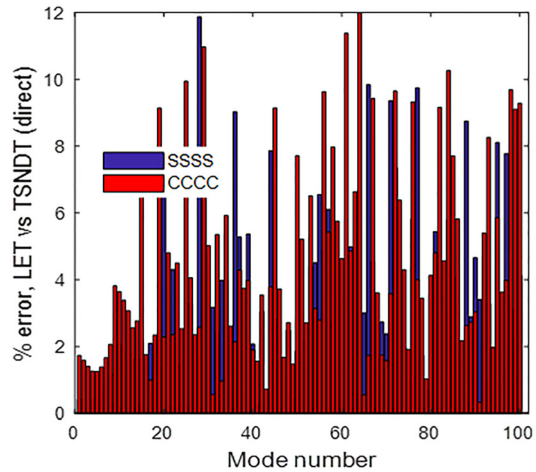

Fig. 3 Total strain energy, in J, from the TSNDT and the 3D LET (left), and the relative error between them (right) for the 80 × 20 × 2 mm SS and clamped plates

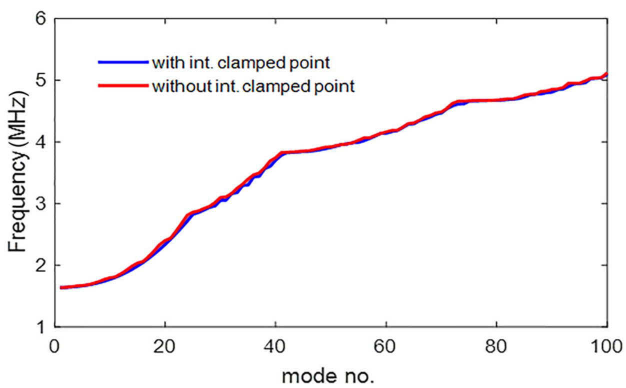

Fig. 4 Frequencies of the first 100 modes of vibration of the $e = 16$ clamped plate with and without internal points constrained

directions. In the TSNDT, it is accomplished by setting $u_{1i}, u_{2i}, u_{3i} = 0, i = 0$ to 3 (see Eq. (9)). As shown in Fig. 1, the plate midsurface to the left (right) of the point P is denoted by R_1 (R_2). For plates with $e = 1$, 4, 16, and 25, we computed results using 40×40, 80×20, 160×10, and 200×8 uniform four-node elements using the TSNDT.

Clamped edges. We have displayed in Fig. 4 frequencies of the first 100 vibration modes of a clamped plate of $e = 16$ with and without the internal constrained points. As in Refs. [30] and [31] where the Kirchhoff theory and the FSDT were used, respectively, in the TSNDT imposing an internal constraint does not affect the first 100 frequencies of a plate. However, constraining internal points strongly affects shapes of modes 2, 4, 5, 10, and 20, depicted in Fig. 5 by using $(X, Y, Z) = (x_1, x_2, x_3)$. We note that for a plate with the internal constrained points, vibrations of either region R_1 or of region R_2 are miniscule. Although mode 5 is essentially unaffected by constraining the internal points, mode shapes of the vibrating region are quite different.

Following Refs. [30] and [31], we quantify mode localization by parameter, β_1, defined by

$$\beta_1 = \frac{\sum_{i=1}^{n} [u]_i^{\mathrm{T}} [k_{\mathrm{el}}]_i [u]_i}{\sum_{i=1}^{N_{\mathrm{el}}} [u]_i^{\mathrm{T}} [k_{\mathrm{el}}]_i [u]_i} \tag{17}$$

where n is the number of elements in the plate region R_1, N_{el} the total number of elements in the plate, $[k_{\mathrm{el}}]$ the element stiffness matrix, and $\boldsymbol{u}$ the vector of nodal displacements in the mass normalized eigen-vector for the ith mode. Thus, β_1 equals the ratio of the total strain energy of the region R_1 to that of the entire plate. The value of β_1 near 0 implies that most of the plate deformation in region R_1 is annulled.

For the first 100 modes of vibration of plates with $e = 1$, 4, 16, and 25, values of β_1 for each mode and the total number of modes for a given value of β_1 are presented in Fig. 6. These results suggest that the value of β_1 strongly depends upon the eccentricity, e, and for $e = 1$, $\beta_1 < 0.27$ for 97 out of the first 100 modes of vibration implying that there is no noticeable mode localization since energies in regions R_1 and R_2 are proportional to their volumes. However, for $e = 25$, for the first 52 modes of vibration, points in either region R_1 or region R_2 are nearly undeformed since for them, β_1 is either near 0 or 1. For $e = 1$, 4, 16, and 25, the number of modes for which β_1 is either essentially 0 or 1, respectively, equals 0, 18, 41, and 52. Thus, as concluded in Refs. [30] and [31], the total number of modes with nearly null deformations increases with an increase in e.

Simply supported edges. In order to decipher whether or not an in-plane mode of vibration localizes in either region R_1 or R_2, we study free vibrations of the rectangular plate of $e = 16$ with and without constraining interior points. Fringe plots of the total displacement magnitude for nine modes, not necessarily consecutive, are presented in Fig. 7 with top views of the plate for modes 1, 3, and 4, and isometric views for other modes. Values of β_1 and the corresponding histogram are exhibited in Fig. 8.

There is essentially no localization of deformation for the plate without any internal point constrained since $\beta_1 \cong 0.2$ for most modes. However, for the plate with internally constrained points, 37 and 5 modes, respectively, have values of β_1 close to either 0 or 1 signifying their localization in one of the two regions. The remaining 58 modes having values different from 0, 0.2, and 1 are partially localized. We note that the mode localization in one region of an in-plane mode of vibration does not completely kill vibration of points in the other region as occurs for the out-of-plane (or bending) vibration modes. For example, in the deformed shape of mode 4 displayed in Fig. 7, in spite of the localization of the mode in region R_1, points in region R_2 significantly deform. The significant difference between vibrations of clamped and SS plates is the existence of a larger number of in-plane modes in the SS plate as compared to that in the clamped plate. Most of these modes are partially localized thus resulting in nonzero strain energies in both regions of the plate, e.g., see mode 4 in Fig. 7.

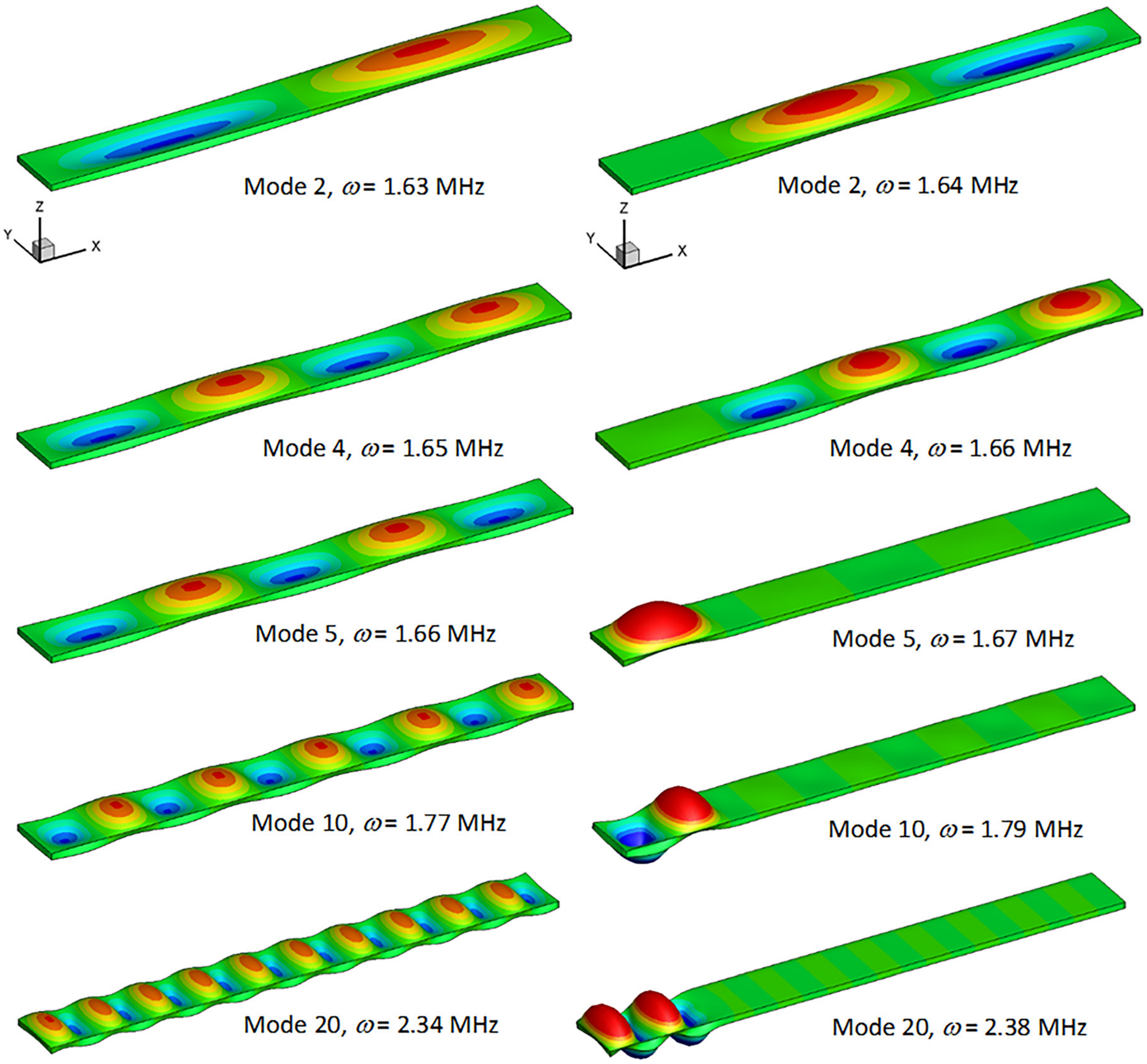

Fig. 5 Mode shapes for free vibration of the clamped plate of $e = 16$ with (right) and without (left) internal constrained points. The red and the blue colors, respectively, represent magnitudes of the maximum positive and the maximum negative transverse displacement. (For references to color in the figure, see the online version.)

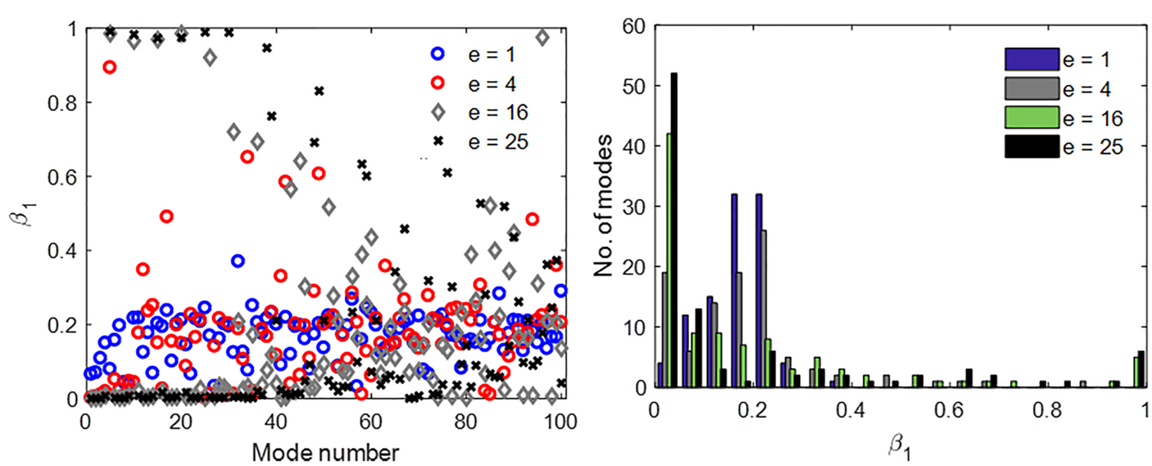

Fig. 6 Mode localization parameter, β_1, for the first 100 modes of vibration of a clamped plate with constrained internal points (left) and distribution of modes over different values of the ratio β_1 for the first 100 vibration modes (right)

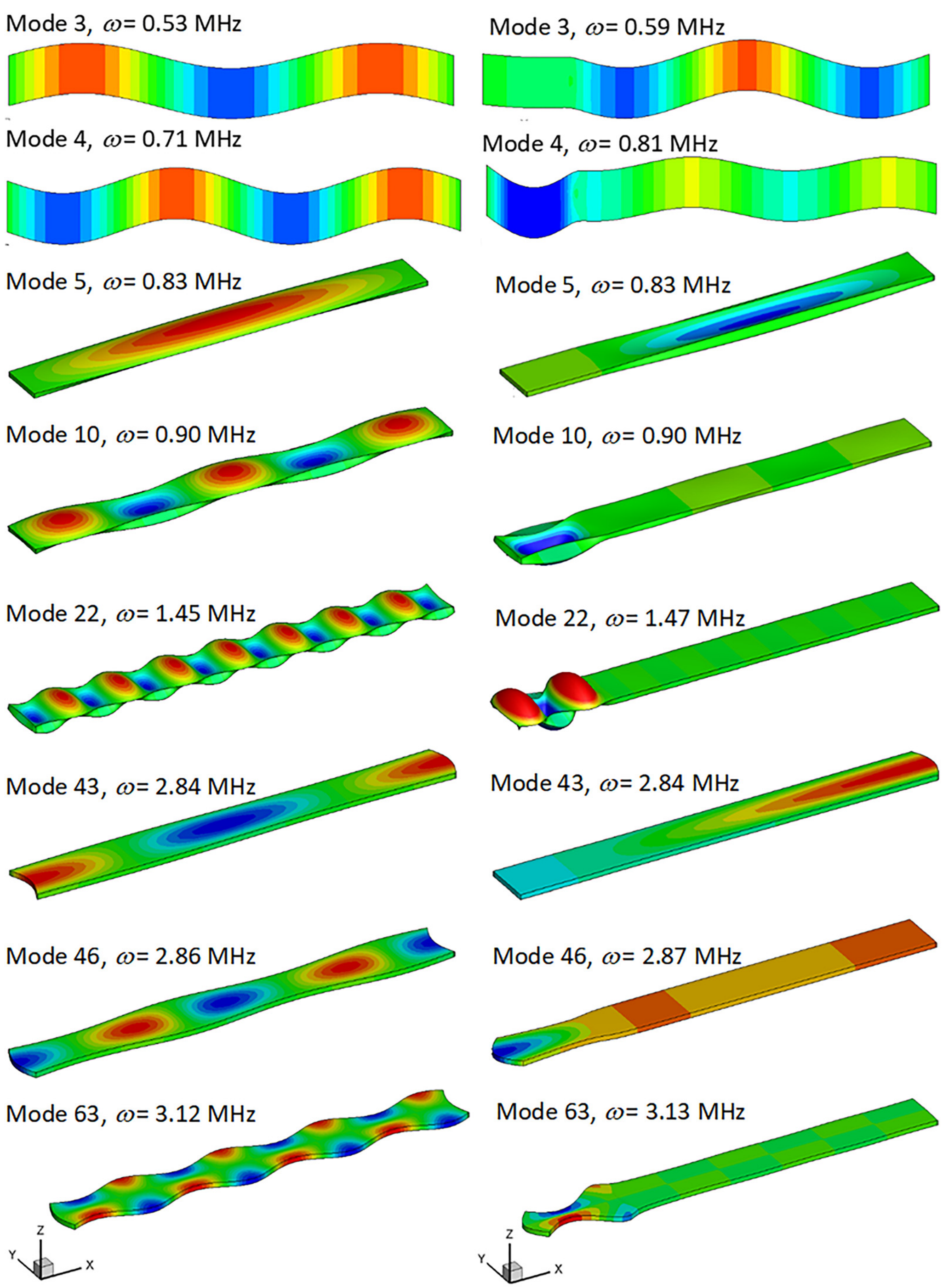

Fig. 7 Fringe plots of the magnitude of the total displacement for different mode shapes of the SS plate of $e = 16$ with (right) and without (left) internal constrained points

Unidirectional Fiber-Reinforced Laminated Plate. We model a unidirectional fiber-reinforced lamina as transversely isotropic with the fiber direction as the axis of transverse isotropy and assign the following values to material parameters:

$$E_L = 140\,\text{GPa}, \quad E_T = E_L/25, \quad G_{LT} = E_L/50, \quad G_{TT} = E_L/125, \quad \nu_{TT} = 0.25, \quad \rho = 5\,\text{g/cc} \tag{18}$$

Here, subscripts L and T, respectively, describe directions parallel and perpendicular (or transverse) to the fiber direction. Material properties with respect to the global coordinate axes are deduced from these by using the tensor transformation rules for stresses and strains.

Clamped edges. For clamped thin rectangular laminates (thickness = length/400) with the axis of transverse isotropy or fiber angle, θ, in all layers of 0 deg, 30 deg, 45 deg, 60 deg, and 90 deg counterclockwise to the global x_1-axis, and eccentricity $e = 20$, we find their first 100 frequencies and the corresponding mode shapes with and without internal points on the line ($l/5$, $b/2$, z) constrained. We note that the elastic moduli with respect to the global coordinate axes depend upon θ. Hence, the global stiffness matrix for the plate varies with the angle θ. Mode shapes for the first and the fifth mode of vibration for three laminae with $\theta = 0$ deg,

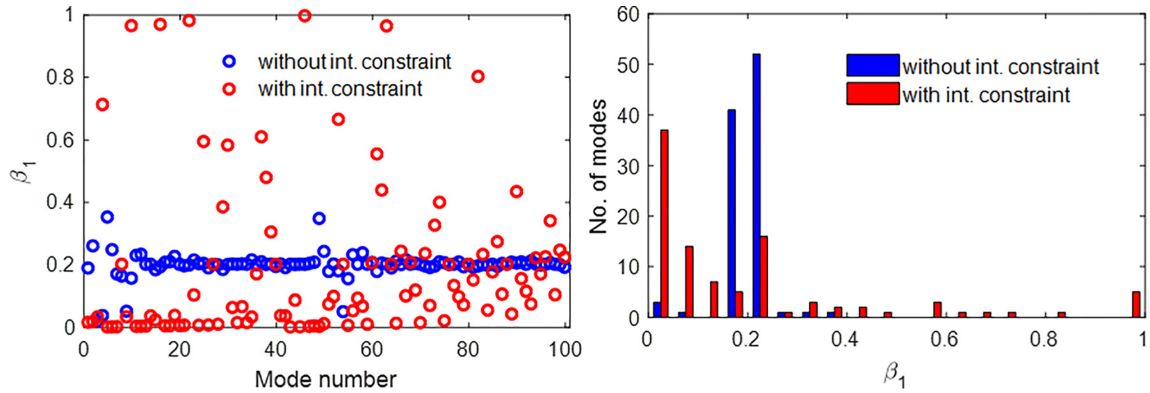

Fig. 8 Values of β_1 for different modes (top) and the histogram of β_1 for the first 100 modes of free vibration of a SS plate of $e = 16$ with (right) and without (left) constraining internal points

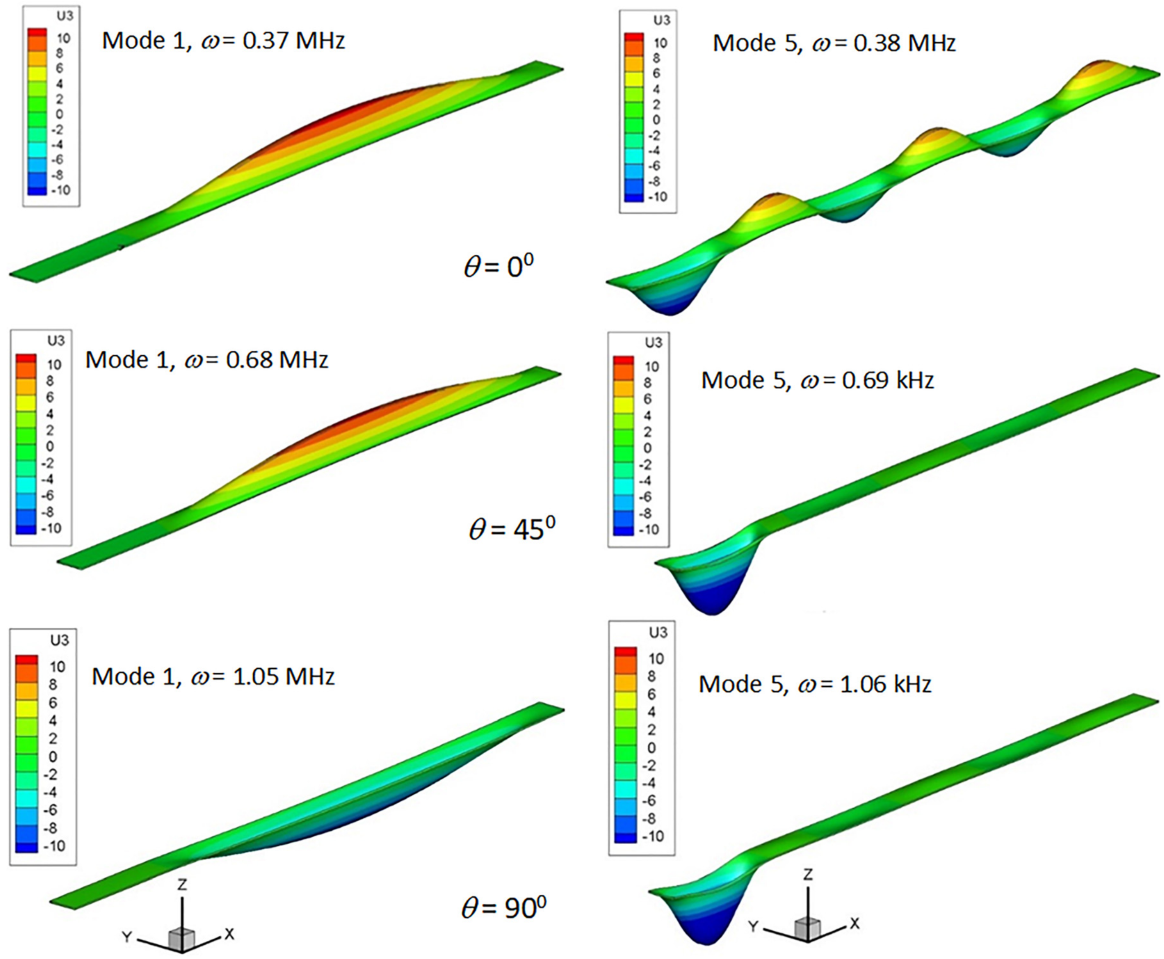

Fig. 9 Mode shapes of mode 1 (left) and mode 5 (right) of vibration of internally constrained clamped rectangular laminae of $e = 20$ for fiber angles of 0 deg, 45 deg, and 90 deg

45 deg, and 90 deg and internally constrained points are presented in Fig. 9. These suggest that the deformation profile for mode 1 (mode 5) is virtually unaffected (significantly influenced) by the fiber orientation angle. For $\theta = 45$ deg and 90 deg, the mode shapes for mode 5 are virtually identical, similar to what was found in Ref. [31] using the FSDT. For the five values of θ, the histograms for the distribution of the mode localization parameter β_1 are given in Fig. 10. In the $\theta = 0$ deg, 45 deg, and 90 deg lamina, the number of modes with $\beta_1 \sim 0.0$ equals, respectively, 30, 44, and 66 (43, 49, and 65) from the FSDT (TSNDT) solution. Thus, the number of modes localized in region R_1 increases with an increase in θ.

Simply supported edges. For SS lamina with $\theta = 0$ deg, 30 deg, 45 deg, 60 deg, and 90 deg and eccentricity $e = 4$, only 7 (23) modes are localized for $\theta = 0$ deg (90 deg) when internal points are constrained. The plate exhibits an interesting behavior for the localization of the in-plane modes of vibration with the change in the fiber orientation angle. In order to see this, we have plotted in Fig. 11 deformed shapes of the plate for the five fiber angles and

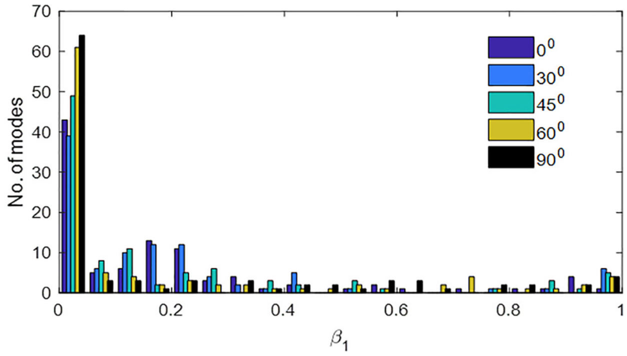

Fig. 10 Histogram of the distribution of β_1 over the first 100 modes of vibration of the internally constrained clamped laminate with different fiber angles

have included fringe plots of the transverse displacement, u_3. We have exhibited in Fig. 12 the top view of the deformed plate for $\theta = 45$ deg, 60 deg, and 90 deg with fringe plots of the in-plane displacement u_2. We see in plots of Fig. 11 that for $\theta = 0$ deg and 30 deg, there is significant transverse displacement as compared to that for $\theta = 45$ deg, 60 deg, and 90 deg. Whereas values of in-plane displacement u_2 are negligible for $\theta = 0$ deg, they are noticeable for $\theta = 45$ deg and 90 deg. Thus, the ratio of energies, β_1, does not correctly represent the mode localization phenomenon for all values of θ. However, for $\theta = 45$ deg and 90 deg, as shown in Fig. 12, the interior constrained points divide the plate into regions R_1 and R_2 one of which has very little deformations as is for isotropic plates.

We observe from results in Fig. 13 that the plate with the 90 deg fibers has 22 localized modes that include both the out-of-plane and the in-plane modes of vibration, and the plate with the 0 deg fibers only 8 modes localized. For the 0 deg (90 deg) plate, $\beta_1 = 0.2$ for 43 (28) modes. Mode shapes for a few modes localized in region R_1 are presented in Fig. 14. We observe that the deformation of mode 14 is partially localized in region R_1, it is similar to that of mode 4 for the isotropic SS plate for which results are shown in Fig. 7. Similarly, partial localization can be seen for mode 17 for which although the deformation localized in R_1, the region R_2 has significant deformations that contribute to the strain energy, and accordingly, β_1 is not close to 0.

Constrained Points on Two Normals for an Isotropic Simply Supported Plate. We now explore the effect of clamping two sets of internal points on mode localization of a SS 80 mm × 20 mm × 2 mm plate with either points (l/5, b/2, z) and (4l/5, b/2, z) or points (l/10, b/2, z) and (4l/5, b/2, z) constrained. The first (second) pair of points is symmetrically (asymmetrically) located about the surface $x_1 = l/2$. Mode shapes for modes 1, 3, and 5 for the first and the second pairs of points are presented in Fig. 15. We conclude from results for the 5th mode of free vibration that for the symmetrically located pair, the deformation is entirely localized in the shorter sections at both ends. However, for the asymmetrically located pair of points, the deformation is entirely localized in the 1/5th of the plate between $x_1 = 0.8l$ and l, and for none of the first 100 modes of vibration, it localized in the (l/10)th of the left end of the plate.

Transient Deformations of Simply Supported Isotropic Plates. In order to ascertain how constraining interior points affects plate's forced vibrations, we study deformations of the 80 mm × 20 mm × 2 mm SS plate ($E = 25$ GPa, $\nu = 0.25$, and $\rho = 5$ g/cc) with and without internally constrained points (l/5, b/2, x_3) by using the 80 × 20 FE mesh of uniform elements, and

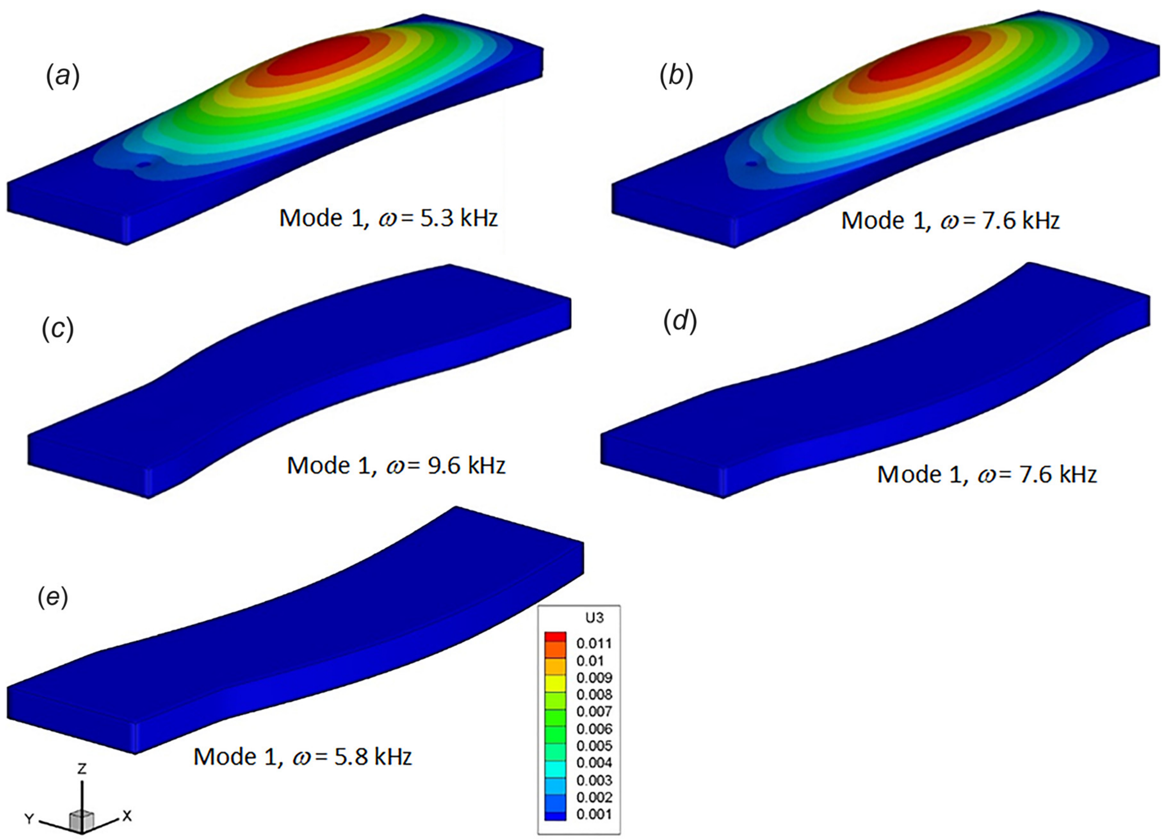

Fig. 11 Fringe plots of the out-of-plane displacement, u_3, for the fundamental mode of vibration of the internally constrained plate with fiber angles of (*a*) 0 deg, (*b*) 30 deg, (*c*) 45 deg, (*d*) 60 deg, and (*e*) 90 deg counter-clockwise to the global x_1-axis. The fringe colors, in the online version of the paper, represent same levels of u_3 (in mm) for each plot.

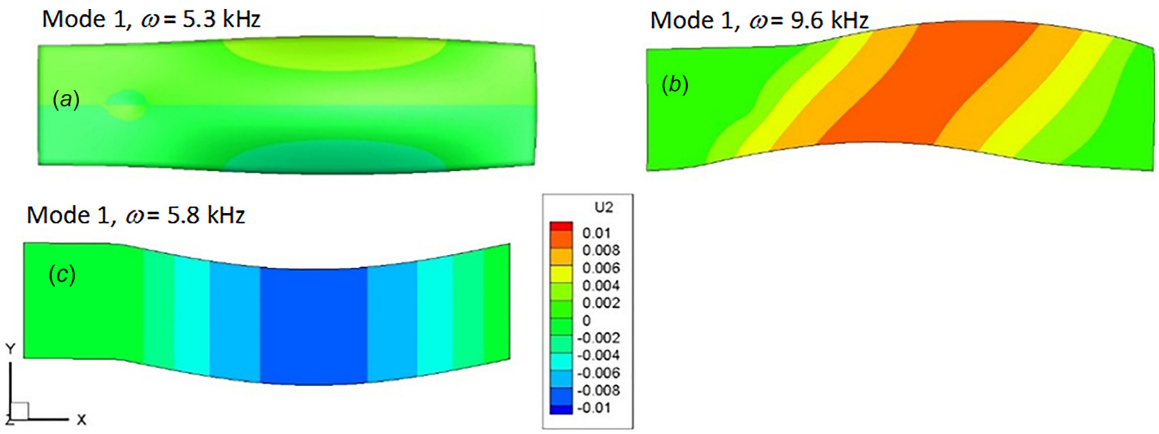

Fig. 12 Top view of the mode shapes and fringe plots of the in-plane displacement, u_2, for fiber angles of (a) 0 deg, (b) 45 deg, and (c) 90 deg. The fringe colors represent same levels of u_2 (in mm) for each plot.

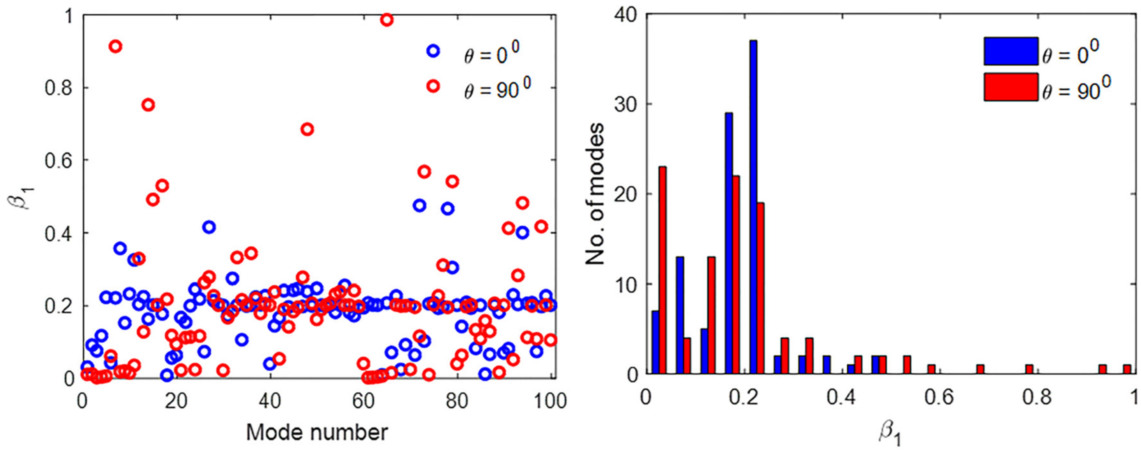

Fig. 13 Distribution of the energy ratio β_1 over the first 100 modes of vibration of the fiber-reinforced lamina with fibers oriented at 0 deg and 90 deg to the global x_1-axis (left), and the corresponding histogram (right)

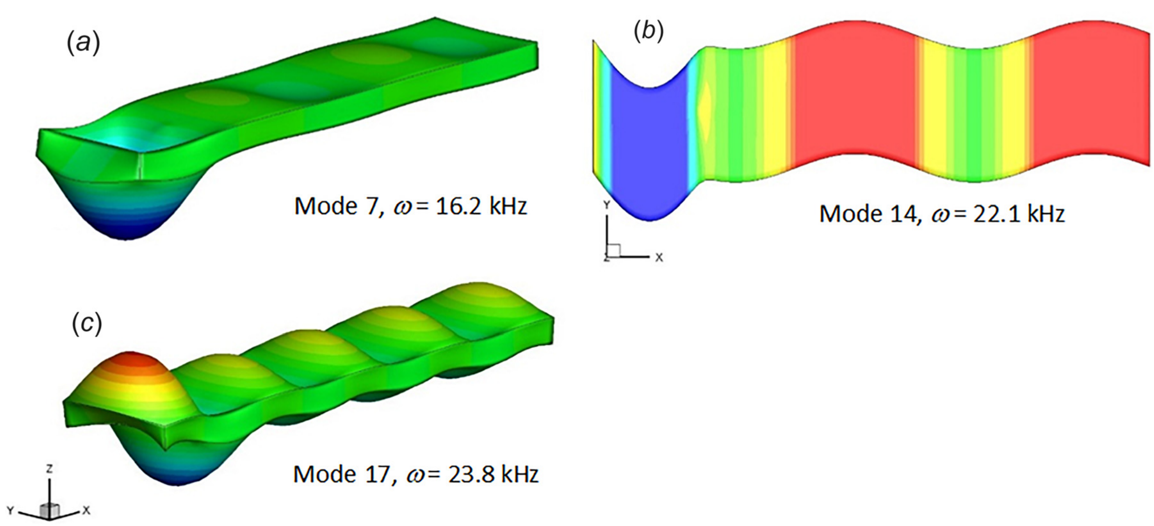

Fig. 14 Localized mode shapes for the 90 deg composite plate: (a) mode 7, (b) top view of mode 14, and (c) mode 17

the time-step = 50 ns that satisfies the stability condition given in Eq. (13). Results for plates with $e = 4$ and 20 were found to be similar. For the plate with $e = 4$, as seen from Fig. 6, mode 6 is localized in region R_2 and modes 1–5 are localized in region R_1. In the first loading scenario, depicted in Fig. 16, the impulsive load on the entire top surface of the plate is nonzero for $0 \leq t \leq 40\ \mu s$ and has either a triangular, or a rectangular or a half sine wave form. Thus, different impulse or linear momentum is

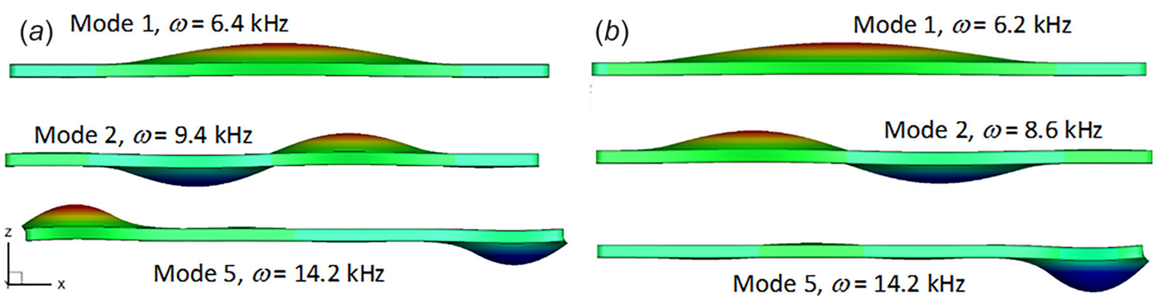

Fig. 15 Shapes of modes 1, 2, and 5 showing deformation localization in the SS plate with two (*a*) symmetrically and (*b*) asymmetrically located pair of constrained points

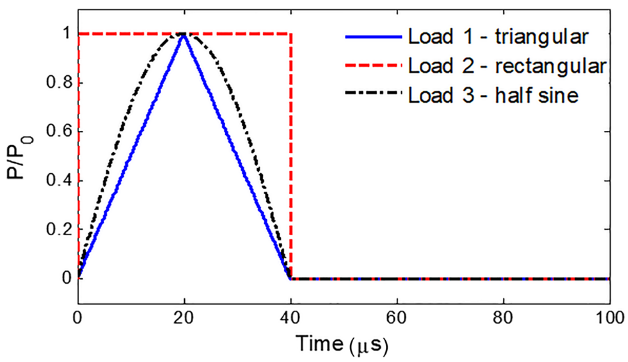

Fig. 16 Three transient impulse loads considered

imparted to the plate for the three loads having possibly different dominant frequencies. In the second scenario, we scrutinize the effect of varying the frequency of the sustained applied sinusoidal load.

We note that an elegant way to analyze a transient problem is to use the mode superposition method that clearly gives the contribution of a mode to the solution. We could not use it here since expressing mode shapes of an internally constrained plate in terms of either polynomials or trigonometric functions is an arduous task.

Impulsive Loads. We have depicted in Fig. 17 time histories of the centroidal deflection and of the strain energy density of regions R_1 and R_2 for the three impulsive loads. It is clear that the loading function only affects the amplitude of the deflection and of the strain energy density, and the two regions vibrate essentially at different frequencies subsequent to the load removal at $t = 40$ μs. The dominant frequencies of vibration of regions R_1 and R_2 found using the fast Fourier transform (FFT) of the time histories of the centroidal deflection correspond, respectively, to those of modes 3 and 1 of the entire plate rather than to those of

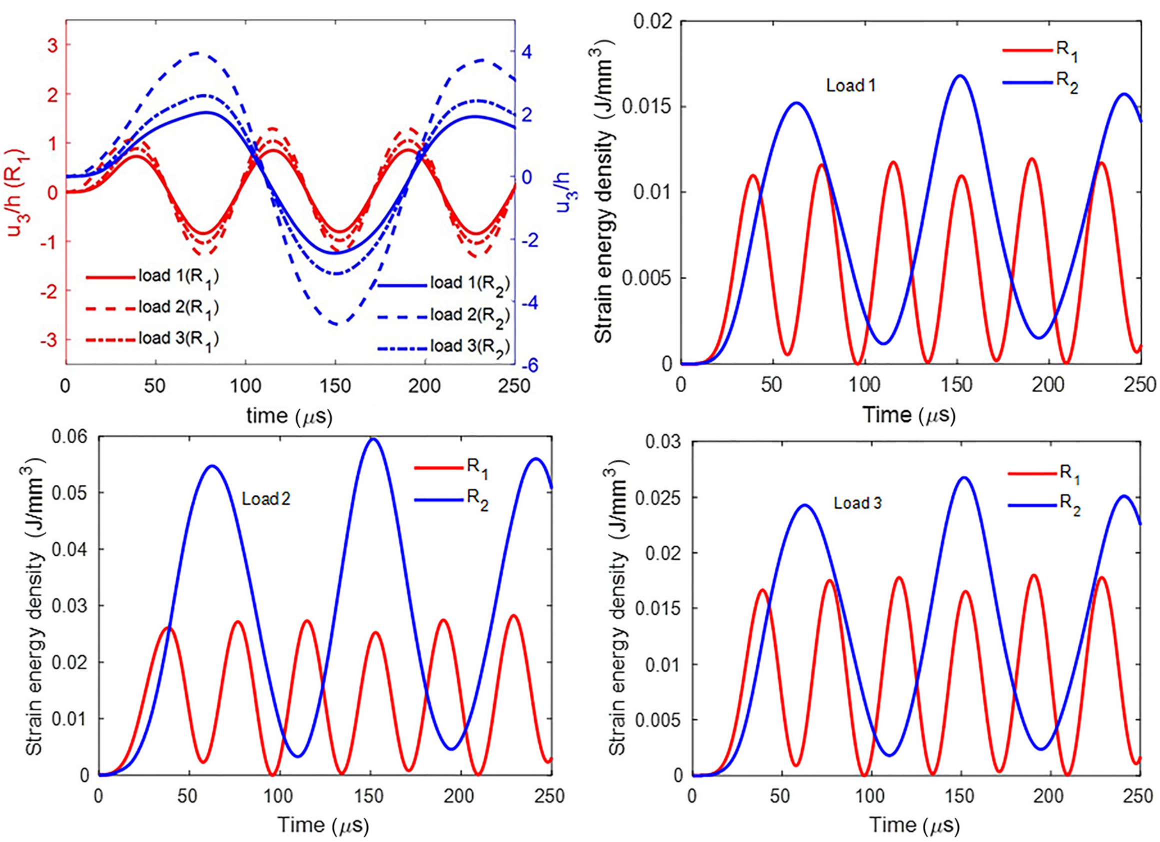

Fig. 17 For the three transient loads, time histories of the centroidal deflection and of the strain energy densities of regions R_1 and R_2 of the plate with internal constrained points

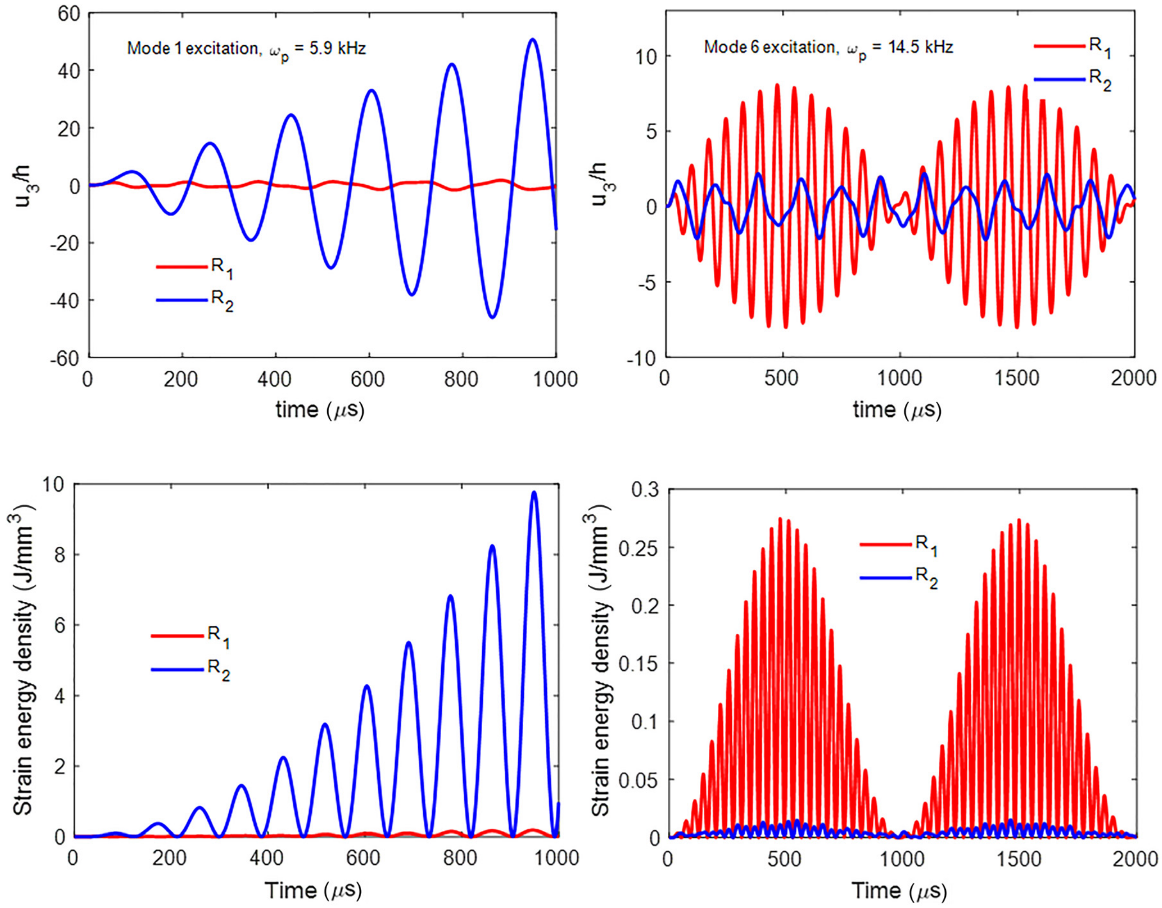

Fig. 18 Time histories of the centroidal deflection and of the strain energy densities of the two regions of the plate for the mode 1 and the mode 6 excitation frequencies

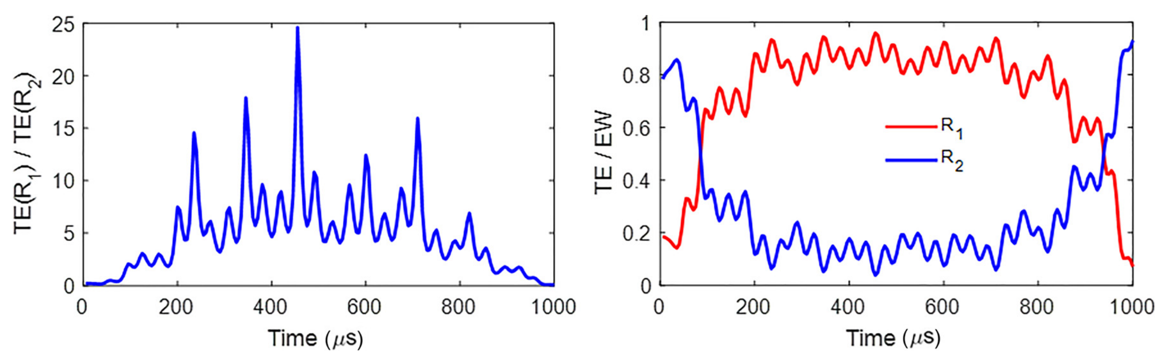

Fig. 19 Time histories of the ratio of the total energy of regions R_1 and R_2 (left) and the ratio of the total energies of each region normalized by the external work done on the entire plate (right)

modes 6 and 1 for which free vibrations get localized in regions R_2 and R_1, respectively. It suggests that for forced vibrations, the two regions deform differently from that for free vibrations.

Sustained Sinusoidal Load on a Rectangular Plate of e = 4. For the pressure load, $P(t) = P_0 \sin(2\pi\omega_p t)$, of frequency ω_p equal to 5.9 and 14.5 kHz for modes 1 and 6 of free vibration of the plate, referred henceforth to as *mode 1 excitation* and *mode 6 excitation frequency*, respectively, we have presented in Fig. 18 time histories of the centroidal displacements and of the strain energy densities of regions R_1 and R_2. We observe that for *mode 1 excitation*, the region R_1 stays nearly at rest as was for free vibration but the amplitude of vibration of region R_2 monotonically increases and its vibrational frequency found by the FFT analysis of its vibrational response equals approximately 5.9 kHz. For the *mode 6 excitation*, the amplitude of vibration of region R_2 stays small but that of region R_1 exhibits beats phenomenon. The FFT analysis of its vibrational response gives the dominant frequency of vibration of region R_1 equal to ~14.5 kHz, i.e., the frequency of mode 6 of free vibration of the entire plate or the excitation frequency of the load, and the region R_2 vibrates at the fundamental frequency, 5.9 kHz, of the plate. The time histories of the ratio of the total energies (TE = kinetic energy + strain energy) of sections R_1 and R_2, and of the ratio of the TE of each region to the cumulative work on the entire plate by external forces, (EW), are presented in Fig. 19. It is observed from these plots that the energy is

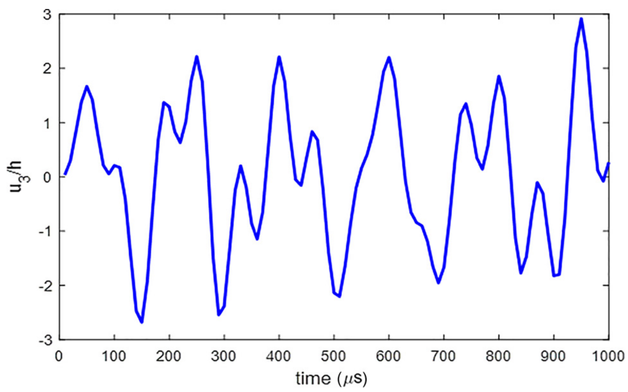

Fig. 20 Centroidal displacement history of an internally unconstrained SS plate under mode 6 harmonic loading

transferred from region R_1 to region R_2 that vibrates at a much lower amplitude. It is supported by the observation that, for the first case, the strain energy of R_1 is negligible as compared to that of R_2, and in the second case, most of the plate deformation is localized in region R_1. This is akin to the response exhibited by the interaction between two pendula of different frequencies explained in textbooks on vibrations (e.g., see Ref. [51]). These results are consistent with Malatkar and Nayfeh's [52] observations of the energy transfer between two widely spaced modes of vibration of a cantilever beam. To delineate the role of the internal constrained points on the phenomenon, the centroidal displacement history of the unconstrained plate under mode 6 excitation is presented in Fig. 20. This knowledge can help design structures subjected to periodic loads for which a smaller substructure that absorbs most of the energy can be sacrificed and the larger substructure saved.

Sustained Sinusoidal Load on a Rectangular Plate of $e = 20$. For the SS plate of $e = 20$, mode 4 (8) is the first transverse mode of

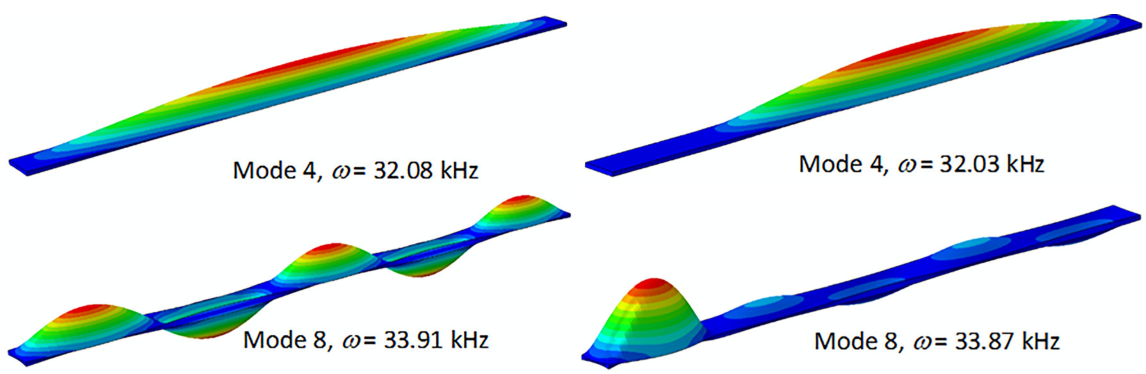

Fig. 21 Mode shapes of transverse vibration for the SS plate of $e = 20$ without (left) and with (right) the internal constraint points

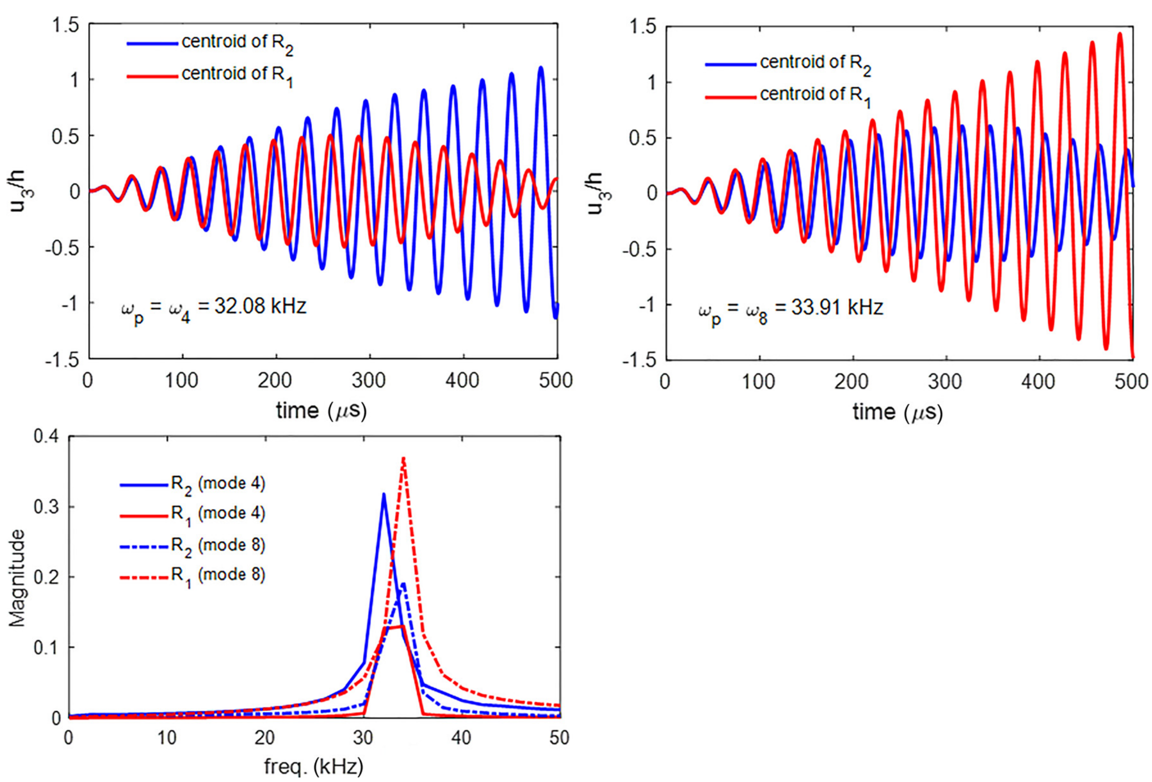

Fig. 22 Displacement histories of centroids of regions R_1 and R_2 under harmonic loads of the two excitation frequencies

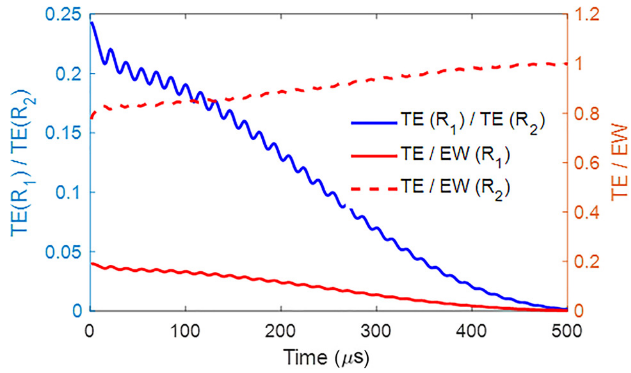

Fig. 23 Time histories of ratio of the total energies of the regions R_1 and R_2 (left) and the ratio of the total energy of each section of the plate to the cumulative external work done on the entire plate

vibration for which the deformation localized in the region R_2 (R_1). The shapes and the corresponding frequencies of modes 4 and 8 of the plate with and without the internal constraint are presented in Fig. 21.

As mentioned earlier for results exhibited in Fig. 4, the addition of the internal constraint does not noticeably affect the frequency of vibration of a particular mode but significantly changes the mode shape. Unlike the plate with $e = 4$ where frequencies of modes 1 and 6 were wide apart, for the plate with $e = 20$, frequencies of the 4th and the 8th modes are close to each other. It is thus likely that the plate would exhibit a different phenomenon under a harmonic excitation of frequency of the 8th mode as compared to that of the $e = 4$ plate under mode 6 excitation. For the pressure load $P(t) = P_0 \sin(2\pi\omega_p t)$ with ω_p (in Hz) as frequencies of modes 4 and 8, of vibration, the time histories of the centroidal displacements of regions R_1 and R_2 and their corresponding FFT are presented in Fig. 22. It is clear that unlike for the $e = 4$ plate, depending on the excitation frequency, a region of the $e = 20$ plate resonates, while the other region exhibits the beat phenomenon due to close values of frequencies of the two modes. Under the mode 4 excitation, the FFT reveals that region R_2 resonates at the mode 4 frequency of 32 kHz, while region R_1 vibrates at approximately 33.5 kHz which is close to the mode 8 frequency. Similarly, for mode 8 excitation, region R_1 resonates at 33 kHz, while region R_2 exhibits beating phenomenon at 32 kHz. The rather flat region in the FFT of region R_1 is because the centroidal deflection was output at 1024 values of time.

From time histories of the ratio of the TE of the two regions and of the ratio of the TE of each region to the external work done, EW, exhibited in Fig. 23, we observed that the TE of region R_1 steadily decreases from 0.25 (ratio of volumes of regions R_1 and R_2) to 0 implying that the total energy of the plate is concentrated in R_2. Similarly, the ratio of the total energy to the EW shows that the TE of the region R_2 gradually increases and that of R_1 decreases. We hypothesize that this is due to the resonance of the region R_2.

In order to delineate effects of internal constraints, the displacement histories of the centroid of the unconstrained plate and the results of the corresponding FFT analyses under the two excitations are presented in Fig. 24. The displacement history of the plate under the mode 4 excitation shows a monotonic increase in the amplitude due to the resonance of the plate. However, for the mode 8 excitation, we see the beating phenomenon since the excitation frequency is close to the fundamental frequency of the plate. This behavior is different from the response of the $e = 4$ unconstrained plate under *mode 6 excitation* where neither the resonance nor the beats phenomenon was observed due to the large difference between the excitation and the fundamental frequencies of the plate. For the $e = 20$ plate, the FFTs of the displacement histories show that the dominant frequency of the plate vibration for the *mode 4 (8) excitation* is about 31 (34) kHz.

Note: For forced vibrations of delaminated plates and laminates studied in Refs. [53] and [54], no localization of deformations was reported. Mode localization has been experimentally and numerically studied in reference [55].

Conclusions

We have numerically studied free and forced vibrations of monolithic and unidirectional fiber-reinforced composite rectangular plates with edges either simply supported or clamped using a TSNDT. Frequencies and strain energies of the first 100 modes of vibration are shown to agree well with those computed using the linear theory of elasticity and the commercial software, ABAQUS. By constraining all points on one or two normals to the midsurface of a plate to have null displacements, the plate deformations are found to localize in one of the two regions separated by the internal constrained points. Significant results from the work include the following:

- When an in-plane mode of vibration is localized, the strain energy of deformations of the other region is not small.
- For rectangular plates with points on two normals constrained from translating in all three directions, the localization occurs simultaneously in two short regions when the constrained points are equidistant from the plate edges.
- A unidirectional fiber-reinforced rectangular plate with internal constrained points switches from a transverse (bending) mode to an in-plane mode of vibration depending on the fiber orientation angle, and both modes exhibit the mode localization phenomenon.

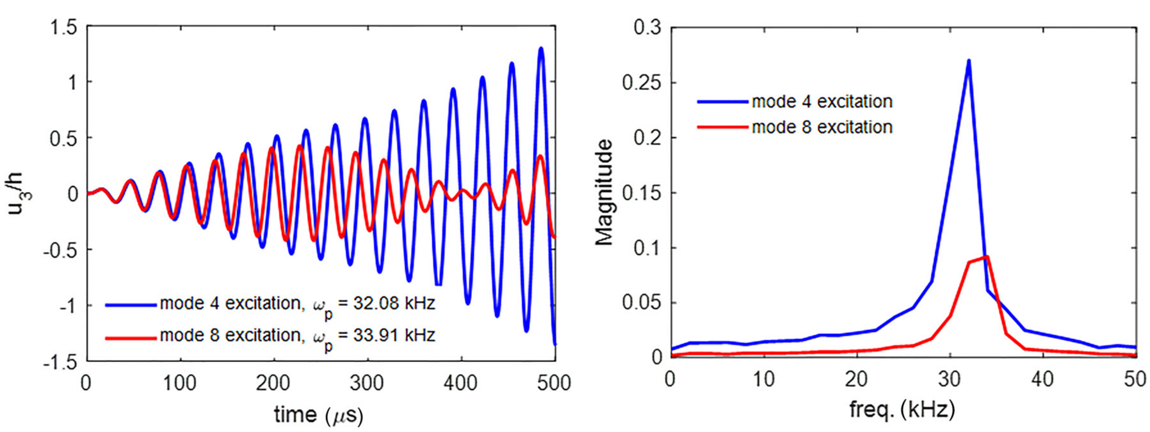

Fig. 24 Centroidal displacement histories of the rectangular plate of $e = 20$ without internal constraints under modes 4 and 8 excitations and the corresponding FFTs of the displacement histories

- For forced vibrations of plates, constraining points on a normal to the plate midsurface divides the plate into two separate sections vibrating at different dominant frequencies. These regions interact with each other through energy transfer resulting in constructive/destructive interference that results in a beating-like phenomenon under suitable loading conditions and plate geometries.
- The mode localization phenomenon can help design cyclically loaded structures so a desired subregion of the structure is significantly deformed, thereby protecting the remainder of the structure and in maximizing energy harvested from them.

Acknowledgment

This work was partially supported by The U.S. Office of Naval Research (ONR) Grant N00014-18-1-2548 to Virginia Polytechnic Institute and State University with Dr. Y. D. S. Rajapakse as the program manager. Views expressed in the paper are those of the authors and neither of ONR nor of Virginia Tech.

References

[1] Anderson, P. W., 1958, "Absence of Diffusion in Certain Random Lattices," Phys. Rev., **109**(5), p. 1492.
[2] Hodges, C., 1982, "Confinement of Vibration by Structural Irregularity," J. Sound Vib., **82**(3), pp. 411–424.
[3] Valero, N., and Bendiksen, O., 1986, "Vibration Characteristics of Mistuned Shrouded Blade Assemblies," ASME J. Eng. Gas Turbines Power, **108**(2), pp. 293–299.
[4] Wei, S.-T., and Pierre, C., 1988, "Localization Phenomena in Mistuned Assemblies With Cyclic Symmetry—Part I: Free Vibrations," ASME J. Vib., Acoust., Stress, Reliab. Des., **110**(4), pp. 429–438.
[5] Bendiksen, O. O., 1987, "Mode Localization Phenomena in Large Space Structures," AIAA J., **25**(9), pp. 1241–1248.
[6] Pierre, C., Tang, D. M., and Dowell, E. H., 1987, "Localized Vibrations of Disordered Multispan Beams-Theory and Experiment," AIAA J., **25**(9), pp. 1249–1257.
[7] Hodges, C., and Woodhouse, J., 1983, "Vibration Isolation From Irregularity in a Nearly Periodic Structure: Theory and Measurements," J. Acoust. Soc. Am., **74**(3), pp. 894–905.
[8] Pierre, C., 1990, "Weak and Strong Vibration Localization in Disordered Structures: A Statistical Investigation," J. Sound Vib., **139**(1), pp. 111–132.
[9] Herbert, D., and Jones, R., 1971, "Localized States in Disordered Systems," J. Phys. C, **4**(10), p. 1145.
[10] Kirkman, P., and Pendry, J., 1984, "The Statistics of One-Dimensional Resistances," J. Phys. C, **17**(24), p. 4327.
[11] Pierre, C., and Plaut, R. H., 1989, "Curve Veering and Mode Localization in a Buckling Problem," Z. Angew. Math. Phys., **40**(5), pp. 758–761.
[12] Nayfeh, A. H., and Hawwa, M. A., 1994, "Use of Mode Localization in Passive Control of Structural Buckling," AIAA J., **32**(10), pp. 2131–2133.
[13] Paik, S., Gupta, S., and Batra, R., 2015, "Localization of Buckling Modes in Plates and Laminates," Compos. Struct., **120**, pp. 79–89.
[14] Ibrahim, R., 1987, "Structural Dynamics With Parameter Uncertainties," ASME Appl. Mech. Rev., **40**(3), pp. 309–328.
[15] Hodges, C., and Woodhouse, J., 1986, "Theories of Noise and Vibration Transmission in Complex Structures," Rep. Prog. Phys., **49**(2), p. 107.
[16] Nowacki, W., 1953, "Vibration and Buckling of Rectangular Plates Simply-Supported at the Periphery and at Several Points Inside," Arch. Mech. Stosow., **5**(3), pp. 437–454.
[17] Gorman, D., 1981, "An Analytical Solution for the Free Vibration Analysis of Rectangular Plates Resting on Symmetrically Distributed Point Supports," J. Sound Vib., **79**(4), pp. 561–574.
[18] Gorman, D., and Singal, R., 1991, "Analytical and Experimental Study of Vibrating Rectangular Plates on Rigid Point Supports," AIAA J., **29**(5), pp. 838–844.
[19] Bapat, A., Venkatramani, N., and Suryanarayan, S., 1988, "A New Approach for the Representation of a Point Support in the Analysis of Plates," J. Sound Vib., **120**(1), pp. 107–125.
[20] Bapat, A., Venkatramani, N., and Suryanarayan, S., 1988, "The Use of Flexibility Functions With Negative Domains in the Vibration Analysis of Asymmetrically Point-Supported Rectangular Plates," J. Sound Vib., **124**(3), pp. 555–576.
[21] Bapat, A., and Suryanarayan, S., 1989, "The Flexibility Function Approach to Vibration Analysis of Rectangular Plates With Arbitrary Multiple Point Supports on the Edges," J. Sound Vib., **128**(2), pp. 209–233.
[22] Bapat, A., and Suryanarayan, S., 1989, "Free Vibrations of Periodically Point-Supported Rectangular Plates," J. Sound Vib., **132**(3), pp. 491–509.
[23] Bapat, A., and Suryanarayan, S., 1992, "The Fictitious Foundation Approach to Vibration Analysis of Plates With Interior Point Supports," J. Sound Vib., **155**(2), pp. 325–341.
[24] Lee, S., and Lee, L., 1994, "Free Vibration Analysis of Rectangular Plates With Interior Point Supports," J. Struct. Mech., **22**(4), pp. 505–538.
[25] Rao, G. V., Raju, I., and Amba-Rao, C., 1973, "Vibrations of Point Supported Plates," J. Sound Vib., **29**(3), pp. 387–391.
[26] Raju, I., and Amba-Rao, C., 1983, "Free Vibrations of a Square Plate Symmetrically Supported at Four Points on the Diagonals," J. Sound Vib., **90**(2), pp. 291–297.
[27] Utjes, J., Sarmiento, G. S., Laura, P., and Gelos, R., 1986, "Vibrations of Thin Elastic Plates With Point Supports: A Comparative Study," Appl. Acoust., **19**(1), pp. 17–24.
[28] Kim, C., and Dickinson, S., 1987, "The Flexural Vibration of Rectangular Plates With Point Supports," J. Sound Vib., **117**(2), pp. 249–261.
[29] Bhat, R., 1991, "Vibration of Rectangular Plates on Point and Line Supports Using Characteristic Orthogonal Polynomials in the Rayleigh-Ritz Method," J. Sound Vib., **149**(1), pp. 170–172.
[30] Filoche, M., and Mayboroda, S., 2009, "Strong Localization Induced by One Clamped Point in Thin Plate Vibrations," Phys. Rev. Lett., **103**(25), p. 254301.
[31] Sharma, D., Gupta, S., and Batra, R., 2012, "Mode Localization in Composite Laminates," Compos. Struct., **94**(8), pp. 2620–2631.
[32] Batra, R., and Aimmanee, S., 2003, "Missing Frequencies in Previous Exact Solutions of Free Vibrations of Simply Supported Rectangular Plates," J. Sound Vib., **265**(4), pp. 887–896.
[33] Du, J., Li, W. L., Jin, G., Yang, T., and Liu, Z., 2007, "An Analytical Method for the in-Plane Vibration Analysis of Rectangular Plates With Elastically Restrained Edges," J. Sound Vib., **306**(3–5), pp. 908–927.
[34] Srinivas, S., and Rao, A., 1970, "Bending, Vibration and Buckling of Simply Supported Thick Orthotropic Rectangular Plates and Laminates," Int. J. Solids Struct., **6**(11), pp. 1463–1481.
[35] Vel, S. S., and Batra, R. C., 1999, "Analytical Solution for Rectangular Thick Laminated Plates Subjected to Arbitrary Boundary Conditions," AIAA J., **37**(11), pp. 1464–1473.
[36] Shah, P., and Batra, R., 2017, "Stress Singularities and Transverse Stresses Near Edges of Doubly Curved Laminated Shells Using TSNDT and Stress Recovery Scheme," Eur. J. Mech.-A, **63**, pp. 68–83.
[37] Lo, K. H., Christensen, R. M., and Wu, E. M., 1977, "A High-Order Theory of Plate Deformation—Part 1: Homogeneous Plates," ASME. J. Appl. Mech., **44**(4), pp. 663–668.
[38] Carrera, E., 1999, "A Study of Transverse Normal Stress Effect on Vibration of Multilayered Plates and Shells," J. Sound Vib., **225**(5), pp. 803–829.
[39] Vidoli, S., and Batra, R. C., 2000, "Derivation of Plate and Rod Equations for a Piezoelectric Body From a Mixed Three-Dimensional Variational Principle," J. Elasticity, **59**(1–3), pp. 23–50.
[40] Batra, R. C., and Vidoli, S., 2002, "Higher-Order Piezoelectric Plate Theory Derived From a Three-Dimensional Variational Principle," AIAA J., **40**(1), pp. 91–104.
[41] Mindlin, R. D., 1951, "Influence of Rotatory Inertia and Shear on Flexural Motions of Isotropic, Elastic Plates," J. Appl. Mech., **18**, pp. 31–38.
[42] Alsuwaiyan, A., and Shaw, S. W., 2003, "Steady-State Responses in Systems of Nearly-Identical Torsional Vibration Absorbers," ASME J. Vib. Acoust., **125**(1), pp. 80–87.
[43] Alsuwaiyan, A. S., 2013, "Localization in Multiple Nearly-Identical Tuned Vibration Absorbers," Int. J. Eng. Technol., **2**(3), p. 157.
[44] Spletzer, M., Raman, A., Wu, A. Q., Xu, X., and Reifenberger, R., 2006, "Ultrasensitive Mass Sensing Using Mode Localization in Coupled Microcantilevers," Appl. Phys. Lett., **88**(25), p. 254102.
[45] Cosserat, E., and Cosserat, F., 1909, "Theorie des Corps Deformables," Paris, A. Hermann and Sons.
[46] Srinivas, S., Rao, C. J., and Rao, A., 1970, "An Exact Analysis for Vibration of Simply-Supported Homogeneous and Laminated Thick Rectangular Plates," J. Sound Vib., **12**(2), pp. 187–199.
[47] Batra, R. C., Vidoli, S., and Vestroni, F., 2002, "Plane Wave Solutions and Modal Analysis in Higher Order Shear and Normal Deformable Plate Theories," J. Sound Vib., **257**(1), pp. 63–88.
[48] Vel, S. S., and Batra, R., 2000, "The Generalized Plane Strain Deformations of Thick Anisotropic Composite Laminated Plates," Int. J. Solids Struct., **37**(5), pp. 715–733.
[49] Hughes, T. J., 2012, *The Finite Element Method: Linear Static and Dynamic Finite Element Analysis*, Courier Corporation, Mineola, NY.
[50] Qian, L., Batra, R., and Chen, L., 2003, "Free and Forced Vibrations of Thick Rectangular Plates Using Higher-Order Shear and Normal Deformable Plate Theory and Meshless Petrov-Galerkin (MLPG) Method," Comput. Model. Eng. Sci., **4**(5), pp. 519–534.
[51] Meirovitch, L., 2001, *Fundamentals of Vibrations*, McGraw-Hill, New York.
[52] Malatkar, P., and Nayfeh, A. H., 2003, "On the Transfer of Energy Between Widely Spaced Modes in Structures," Nonlinear Dyn., **31**(2), pp. 225–242.
[53] Hirwani, C. K., Panda, S. K., and Mahapatra, T. R., 2018, "Nonlinear Finite Element Analysis of Transient Behavior of Delaminated Composite Plate," ASME J. Vib. Acoust., **140**(2), p. 021001.
[54] Xiao, J., and Batra, R., 2014, "Delamination in Sandwich Panels Due to Local Water Slamming Loads," J. Fluids Struct., **48**, pp. 122–155.
[55] Sapkale, S. L., Sucheendran, M. M., Gupta, S. S., and Kanade, S. V., 2018, "Vibroacoustic Study of a Point-Constrained Plate Mounted in a Duct," J. Sound Vib., **420**, pp. 204–226.